An Accurate and Efficient Entire-Domain Basis Galerkin's Method for the Integral Equation Analysis of Integrated Rectangular Dielectric Waveguides

G. Athanasoulias, *Student Member, IEEE,* and N. K. Uzunoglu, *Member, IEEE*

Abstract—**The propagation characteristics of multiple coupled rectangular dielectric waveguides are investigated through an integral equation analysis. In contrast with the widely used subdomain-basis Galerkin's method, in this work a novel set of entire-domain basis functions is introduced. This set consists of plane wave functions that satisfy Maxwell's equations in each guiding region, therefore representing a proper expansion system. The simple form of the basis functions employed enables the accurate numerical evaluation of the spectral integrals, by means of an efficient asymptotic extraction technique. It is found that the computed dispersion curves presented for various single and coupled waveguides compare very favorably to published results of other methods. Finally, leakage effects in lossy waveguides are numerically treated for the first time, in view of mode transitions from leaky to bound regime. The technique presented in this paper is accurate, though conceptually simple, and can deal with a wide variety of integrated circuits and multilayered substrate configurations. It is also demonstrated that its main advantage is superior computational efficiency, since very satisfactory results are obtained with only a few expansion terms.**

I. Introduction

THE RECTANGULAR dielectric waveguide (RDW) [1], being the fundamental building block of several components, plays a very important role in the field of integrated optics [2]. Practical integrated transmission lines like rib and channel guides, as well as directional couplers, are constructed by immersing one or more RDW's within a layered dielectric surround. In these devices, the RDW provides the transmission medium to confine and direct optical signals. The rapid development of millimeter and submillimeter-wave monolithic integrated circuit technology has also extended its potential applications to lower frequency regions [3].

Techniques for analyzing dielectric waveguides have been well-addressed in the literature. Among the more rigorous techniques, we mention finite element methods [4], mode matching methods [5]–[6], variational methods [7] and electric field integral equation (EFIE) methods [8]–[16]. Since EFIE's are the subject of this paper, a more detailed overview of these methods is presented. The EFIE in its standard form, also referred to as domain-integral equation, considers the RDW domains as local perturbations of the configuration, replacing them with equivalent polarization currents [8], [9]. Then, the electric dyadic Green's function is used for the integral representation of the field in the layer in which the RDW's are embedded [10]. Because of their rigorous full wave formulation, EFIE's are capable of treating both open and closed structures and describing physical effects like mode leakage. It should be mentioned that different approaches have also appeared in the literature. In [11], a boundary integral equation is developed, while in [12] higher-order boundary conditions are enforced to derive an equivalent one-dimensional integral equation.

In this paper, the standard EFIE is employed and is subsequently solved using Galerkin's method. Most of the existing implementations of this method are based on the use of pulse subdomain basis functions [9], [10], that require a fine segmentation of the guide cross-section. As a consequence, a large number of unknowns is introduced, which renders the results either unstable or numerically costly [12], [13]. Furthermore, a subsectional expansion is not proper from physical point of view, since the discontinuous variation of the electric field creates fictitious charges and currents on the boundaries of the subdomains. In order to overcome the aforementioned drawbacks, a novel set of entire-domain basis functions appropriate for RDW's is developed. This set is constructed by discretizing an exact integral representation of the electric field inside each guiding region. The simple plane wave functions derived satisfy Helmholtz's equation, therefore representing a physical expansion mechanism, valid for both lossy and lossless materials. Even though the modeling of RDW's with entire-domain expansion terms has been suggested elsewhere [8], [13], [15], the systematic implementation of plane wave basis functions for the solution of the EFIE is believed to be new. Besides the accuracy and the simplicity of the proposed method, its major advantage lies in its numerical efficiency, since very satisfactory results can be obtained using only a few expansion terms. Waveguides of more complicated cross-sections can also be analyzed, provided that they can be decomposed into a number of RDW's.

In Section II of this paper, the general formulation of the problem is presented. A set of entire-domain basis functions for the modeling of RDW's is introduced in Section III and Galerkin's method is applied. In Section IV, the elements of

Manuscript received February 27, 1995; revised July 10, 1995.

The authors are with the Department of Electrical and Computer Engineering, National Technical University of Athens, GR-106 82, Athens, Greece.

IEEE Log Number 9415479.

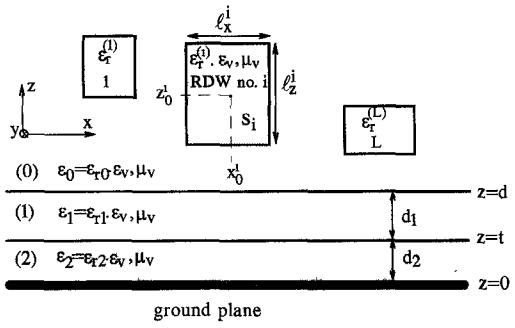

Fig. 1. Cross-sectional view of the configuration of L RDW's positioned above a grounded double dielectric layer substrate.

the coefficient matrix are derived in terms of infinite spectral integrals. In order to compute these integrals accurately and efficiently, an asymptotic extraction technique is developed and demonstrated. Finally, in Section V some numerical results are presented for coupled RDW's of both equal and unequal size, and are compared with published results of other methods. Leakage characteristics of a strip dielectric guide are also examined and special emphasis is placed on the investigation of leakage phenomena in lossy waveguides. Three appendices provide details on the derivation of the basis functions and the evaluation of the elements of the system matrix.

II. Formulation of the Problem

The geometrical configuration and coordinate system of the waveguide considered in the analysis are depicted in Fig. 1. The whole structure is assumed to be uniform along the propagation direction y. The guiding region consists of a number L of rectangular dielectric waveguides (RDW), that are in turn embedded in layer (0) of a planar stratified background medium. This can be any layered configuration with or without ground planes, or it can be an enclosed partially filled waveguide geometry. For simplicity, Fig. 1 shows a grounded double layer substrate, where domain (0) in which the RDW's are located is semiinfinite.

The position of the ith RDW with width ℓ_x^i and height ℓ_z^i is defined by its cross-section center coordinates (x_0^i, z_0^i),while its constant relative permittivity is denoted by $\varepsilon_r^{(i)}$. The homogeneous domains (0), (1), and (2) of the surrounding are also characterized by their relative permittivities $\varepsilon_{r0}, \varepsilon_{r1}$, and ε_{r2}, respectively. All media are assumed nonmagnetic. Symbols ε_v and μ_v stand for the electric and magnetic constants in vacuum. To include losses, the permittivities are considered to be complex in general. A wide variety of practical integrated circuits can be constructed from the topology of the waveguide described above by changing the number L of RDW's and their geometrical and electrical parameters.

In the absence of external sources, time-harmonic solutions of the Maxwell's equations in the structure of Fig. 1 are sought by considering the electric fields in the domain of the RDW's as equivalent polarization currents [8]–[9]. Omitting the $\exp(j\omega t)$ time factor, the electric field in layer (0) can be written in an integral form [10] with kernel the dyadic Green's function $\overline{\overline{G}}(\overline{r}, \overline{r}')$, as

$$\overline{E}(\overline{r}) = k_v^2 \sum_{i=1}^{L} \delta\varepsilon_{ri} \iiint_{V_i} \overline{\overline{G}}(\overline{r}, \overline{r}') \cdot \overline{E}(\overline{r}')\, dV(\overline{r}') \quad (1)$$

where $\delta\varepsilon_{ri} = \varepsilon_r^{(i)} - \varepsilon_{r0}, k_v = \omega\sqrt{\varepsilon_v\mu_v}$ and V_i is the space occupied by the ith RDW. Integration in (1) must be performed in the principal value sense [17], in which an exclusion principal volume needs to be specified. This concept is inherent [18] in the following spectral representation of $\overline{\overline{G}}(\overline{r}, \overline{r}')$

$$\overline{\overline{G}}(\overline{r}, \overline{r}') = \frac{1}{(2\pi)^2} \iint_{-\infty}^{\infty} \overline{\overline{g}}(k_x, k_y; z, z') \cdot e^{j(k_x(x-x)+k_y(y-y'))}\, dk_x\, dk_y - \frac{\hat{z}\hat{z}}{k_0^2}\delta(\overline{r} - \overline{r}'). \quad (2)$$

The first term on the right-hand side of (2) is the eigenfunction representation of the principal value part of $\overline{\overline{G}}(\overline{r}, \overline{r}')$, with a disk-shaped exclusion volume, while the delta-function term corresponds to the depolarizing dyad [17]–[18].

The spectral dyad $\overline{\overline{g}}(k_x, k_y; z, z')$ in (2) can be derived using well known procedures [10], [19] and, as usual, it decomposes into a primary and a secondary part ($\overline{\overline{g}} = \overline{\overline{g}}^{\text{sec}} + \overline{\overline{g}}^{\text{pr}}$). The explicit forms pertaining to the geometry of Fig. 1 are given by

$$\overline{\overline{g}}^{\text{pr}}(k_x, k_y; z, z') = \overline{\overline{g}}_2(k_x, k_y)e^{jk_{z0}(z-z')}u(z'-z) + \overline{\overline{g}}_3(k_x, k_y)e^{-jk_{z0}(z-z')}u(z-z') \quad (3a)$$

$$\overline{\overline{g}}^{\text{sec}}(k_x, k_y; z, z') = \overline{\overline{g}}_1(k_x, k_y)e^{-jk_{z0}(z+z')} \quad (3b)$$

where

$$\overline{\overline{g}}_{2(3)} = \frac{-j}{2k_0^2 k_{z0}} \begin{bmatrix} k_0^2 - k_x^2 & -k_x k_y & \mp k_x k_{z0} \\ -k_x k_y & k_0^2 - k_y^2 & \mp k_y k_{z0} \\ \mp k_x k_{z0} & \mp k_y k_{z0} & k_\rho^2 \end{bmatrix} \quad (4)$$

$$\overline{\overline{g}}_1 = \frac{-j}{2k_0^2 k_{z0}} \left\{ R^{\text{TE}} \begin{bmatrix} +k_0^2 k_y^2/k_\rho^2 & -k_x k_y k_0^2/k_\rho^2 & 0 \\ -k_x k_y k_0^2/k_\rho^2 & +k_0^2 k_x^2/k_\rho^2 & 0 \\ 0 & 0 & 0 \end{bmatrix} + R^{\text{TM}} \begin{bmatrix} -k_x^2 k_{z0}^2/k_\rho^2 & -k_x k_y k_{z0}^2/k_\rho^2 & k_x k_{z0} \\ -k_x k_y k_{z0}^2/k_\rho^2 & -k_y^2 k_{z0}^2/k_\rho^2 & k_y k_{z0} \\ -k_x k_{z0} & -k_y k_{z0} & k_\rho^2 \end{bmatrix} \right\}. \quad (5)$$

In (3a), $u(\pm(z-z'))$ denotes the unit step function. The following parameters and functions have also been introduced

$$k_0 = k_v\sqrt{\varepsilon_{r0}}, \quad k_\rho^2 = k_x^2 + k_y^2, \quad k_{z0} = \sqrt{k_0^2 - k_\rho^2}. \quad (6)$$

The branch cut of the double valued square root k_{z0} is chosen to lie along the line $\text{Im}(k_{z0}) = 0$, and the proper Riemann sheet is defined by requiring $\text{Im}(k_{z0}) < 0$ [20]. Equations (3b) and (5) apply for structures in which the region (0) is semiinfinite. The effects of the layered substrate are incorporated into the formulation (5) through the spectral reflection coefficients R^{TE} and R^{TM} of TM and TE waves that are incident upon the boundary at $z = d$ from region

(0). The analytical expressions of R^{TM} and R^{TE} are given in Appendix A for configurations with or without a ground plane at $z = 0$ (Fig. 1). Due to shortage of space, the secondary dyad of covered structures is not included in the paper.

The analysis is next devoted to the investigation of guided modes of the form $\overline{E}(\overline{r}) = \overline{e}(\overline{\rho})e^{-j\beta y}$, where β is the propagation constant along the y direction and $\overline{\rho} = x\hat{x} + z\hat{z}$. We denote by $\overline{e}_i(\overline{\rho})$ the field on the cross-section S_i of the ith RDW, i.e., $\overline{e}_i(\overline{\rho}) = \overline{e}(\overline{\rho}), \overline{\rho} \in S_i$. In this case, (1) in conjunction with (2) reduces to

$$\overline{e}_j(\overline{\rho}) + \frac{k_v^2}{k_0^2}\delta\varepsilon_{rj}\hat{z}e_{jz}(\overline{\rho}) = \frac{k_v^2}{2\pi}\sum_{i=1}^{L}\delta\varepsilon_{ri}\iint_{S_i} dx'\,dz' \cdot \left(\int_{-\infty}^{\infty} dk_x\, e^{jk_x(x-x')}\overline{\overline{g}}(k_x,-\beta;z,z')\right)\cdot\overline{e}_i(\overline{\rho}'), \quad \overline{\rho}\in S_j. \tag{7}$$

The field $\overline{e}_j(\overline{\rho})$ on the jth RDW, increased by the source dyadic term (left-hand side), is thus expressed as superposition of fields contributed by the polarization currents $(j\omega\delta\varepsilon_{ri}\overline{e}_i(\overline{\rho}))$ in all the RDW's (right-hand side).

If (7) is written for $j = 1, 2, \cdots, L$ a coupled system of L integral equations is formed for the unknown field distributions $\overline{e}_i(\overline{\rho}), i = 1, 2, \cdots, L$. It should be mentioned that this system is quite general in the sense that no assumption has been made for the number L of the RDW's and their positions. Furthermore, the cross-section of the guiding regions need not be rectangular in shape. In the next section, we turn to a Galerkin's solution of the system in (7) using entire-domain basis functions.

III. Entire-Domain Basis Galerkin's Solution

The effectiveness of a method of moments numerical solution for (7) depends on a judicious choice of basis functions. These functions should incorporate as closely as possible the physical conditions of the actual electric field on the cross-sections S_i of the RDW's (Fig. 1). In this work, instead of using subdomain functions, we employ entire-domain basis functions for expanding the unknown fields and for testing the results (Galerkin's method). The first step in the development of a proper set of expansion terms, is to enforce the electric field $\overline{e}_i(\overline{\rho})$ to satisfy the appropriate homogeneous Helmholtz equation. It is found (Appendix B) that in the source-free region of the ith RDW the following integral representation holds

$$\overline{e}_i(x,z) = \int_0^{2\pi}\exp(ju_i(\beta)[(\cos\phi_k(z-z_0^i) + \sin\phi_k(x-x_0^i)]) \cdot \overline{C}_i(\phi_k)\,d\phi_k, \qquad (x,z)\in S_i \tag{8}$$

where

$$k^{(i)} = k_v\sqrt{\varepsilon_r^{(i)}}, \quad u_i(\beta) = \sqrt{(k^{(i)})^2 - \beta^2}. \tag{9}$$

The representation in (8) expresses the electric field in the ith RDW as a bundle of waves with wavenumbers $u_i(\beta)$, amplitudes $\overline{C}_i(\phi_i)$, and directions varying from $\phi_k = 0$ to $\phi_k = 2\pi$. This concept has first been dealt with in [21], where a general proof is given for solutions of Laplace's equation. It is pointed out that (8) also applies for lossy structures and leaky modes, cases in which the factor $u_i(\beta)$ of (9) is complex.

Equation (8) can be utilized to develop entire-domain basis functions for the unknown field $\overline{e}_i(\overline{\rho})$ on the cross section S_i. To this end, the integral in (8) is discretized and it is approximated by a finite summation over N_i angles ϕ_{kn}^i in the range $[0, 2\pi]$. This set of spectral angles may be chosen according to the following rule

$$\phi_{in} \equiv \phi_{kn}^i = \phi_{i0} + \frac{2\pi}{N_i}(n-1), \qquad n = 1, 2, 3, \cdots, N_i \tag{10}$$

where the offset angle ϕ_{i0} is usually zero. When convergence in the solutions is reached by using sufficiently large numbers N_i in the angular sampling (see Section V), the results are insensitive to this offset.

Next we set

$$k_{xn}^i = u_i(\beta)\sin(\phi_{in}), \quad k_{zn}^i = u_i(\beta)\cos(\phi_{in}), \quad \overline{C}_{in} = \overline{C}_i(\phi_{in}) \tag{11a}$$

$$f_{in}(x,z) = f_{in}^x(x)\cdot f_{in}^z(z), \quad f_{in}^x(x) = e^{jk_{xn}^i(x-x_0^i)}, \quad f_{in}^z(z) = e^{jk_{zn}^i(z-z_0^i)}. \tag{11b}$$

Finally, the electric field $\overline{e}_i(\overline{\rho})$ is expressed in terms of N_i basis functions as

$$\overline{e}_i(x,z) = \sum_{n=1}^{N_i}\overline{C}_{in}f_{in}(x,z) = \sum_{a=x,y,z}\sum_{n=1}^{N_i}\hat{a}C_{in}^a f_{in}(x,z), \qquad (x,z)\in S_i. \tag{12}$$

It has therefore been introduced through (10)–(12) a novel set of entire-domain basis functions, appropriate for RDW's. This set constitutes a proper expansion mechanism, since its members satisfy the homogeneous vector wave equation. A remarkable and unique feature of these functions is their explicit dependence on the wavenumber β, through the term $u_i(\beta)$ of (9).

In the Galerkin's method of solution, the expansion field of (12) is substituted into the system of integral equations (7) and the result is tested with $\hat{s}f_{jm}^*(\overline{\rho})$. This means that the inner products of both parts of (7) with $\hat{s}f_{jm}^*(\overline{\rho})$ are integrated over the cross section S_j. The asterisk (*) denotes complex conjugate. The above procedure is applied for $j = 1, 2, \cdots, L, m = 1, 2, \cdots, N_j$, and $s = x, y, z$. Thus, an homogeneous algebraic system of equation is formed with unknown functions the field coefficients C_{in}^a for $i = 1, 2, \cdots, L, n = 1, 2, \cdots, N_i$, and $a = x, y, z$. This system can be written symbolically as

$$\sum_{i=1}^{L}\sum_{n=1}^{N_i}\sum_{a=x,y,z}F_{mn}^{sa}(j,i)C_{in}^a = 0 \tag{13a}$$

and in a more compact form

$$\overline{\overline{F}}\cdot\overline{C} = 0. \tag{13b}$$

The total number of unknowns is N_{tot} and the order of the system matrix $\overline{\overline{F}}$ is $N_{\text{tot}} \times N_{\text{tot}}$, where

$$N_{\text{tot}} = 3 \cdot (N_1 + N_2 + \cdots + N_L). \tag{14}$$

The analytical expressions of the elements $F^{sa}_{mn}(j,i)$ of the system are given in the next section. To obtain a nontrivial solution in (13), the determinant of the coefficient matrix $\overline{\overline{F}}$ must vanish, leading to discrete solutions for the propagation constant β.

In constructing the set of basis functions (11), Gauss' law has not been used yet. If we impose this law on the field of (12), we obtain

$$\nabla \cdot (\bar{e}_i(x,z)e^{-j\beta y}) = 0 \Rightarrow k^i_{xn}C^x_{in} + k^i_{zn}C^z_{in} - \beta C^y_{in} = 0, \qquad n = 1,2,\cdots,N_i. \tag{15}$$

Using the above condition, (13) is rewritten as

$$\sum_{i=1}^{L}\sum_{n=1}^{N_i}\left\{\left[F^{sx}_{mn}(j,i) + \frac{k^i_{xn}}{\beta}F^{sy}_{mn}(j,i)\right]C^x_{in} + \left[F^{sz}_{mn}(j,i) + \frac{k^i_{zn}}{\beta}F^{sy}_{mn}(j,i)\right]C^z_{in}\right\} = 0. \tag{16}$$

Thus, the number of unknown field coefficients in the ith RDW reduces from $3N_i$ to $2N_i$ and the new system matrix is formed by selecting [13] the transverse components ($s = x, z$) of (16). The validity of the above procedure is ensured by the fact that the transverse components of the EFIE (7) yield a unique description of the guided wave modes [14].

The analysis presented above can easily be modified to accommodate, in an elegant manner, structures that are characterized by certain planes of symmetry. Consider for example the configuration (Fig. 6(a)) of two identical RDW's that are symmetrically located about the y-z plane. In this case, a magnetic or an electric wall can be placed at the plane of symmetry without affecting the field distributions. The modes are then designated as even or as odd modes. The symmetry properties of the electric field can be explicitly incorporated into the sets of basis functions used. Let N_1 denote the number of basis functions in the left RDW ($i = 1$) for which the expansion angles ϕ_{1n} are selected according to (10). For its symmetrical RDW ($i = 2$) we choose $N_2 = N_1$ and set $\phi_{2n} = 2\pi - \phi_{1n}$. Then, it follows from (11) that $f_{2n}(x,z)$ is the reflection of $f_{1n}(x,z)$ with respect to the plane $x = 0$. Eventually, by setting $C^a_{2n} = \pm C^a_{1n}$ [10], we can specify even or odd modes. As a consequence, the testing procedure of Galerkin's method needs only be applied for the first RDW ($j = 1$).

IV. Manipulation of the Spectral Integrals

A. Analysis

In this section, the final forms of the elements $F^{sa}_{mn}(j,i)$ of the coefficient matrix are given. In order to keep the formalism simple and avoid lengthy equations, only the key results are presented. For convenience, the term $\delta\varepsilon_{ri}$ in (7) is incorporated into the unknown field coefficients C^a_{in}. After a straightforward algebraic manipulation, the elements $F^{sa}_{mn}(j,i)$ are derived successively as

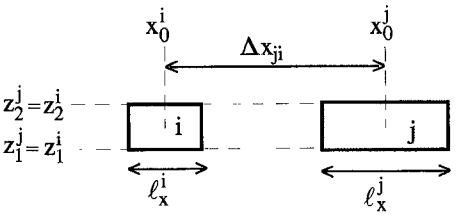

Fig. 2. Geometrical configuration of a pair (j,i) of RDW's for which the primary integrands of (21) decrease as $1/k^2_x$.

$$F^{sa}_{mn}(j,i) = E^{sa}_{mn}(j,i) - D^{sa}_{mn}(j,i) \tag{17}$$

$$D^{sa}_{mn}(j,i) = \frac{1}{\delta\varepsilon_{ri}}\left(1 + \frac{k^2_v}{k^2_0}\delta\varepsilon_{ri}\delta_{sz}\right)\delta_{ij}\delta_{sa}A_{mn}(j) \tag{18}$$

$$E^{sa}_{mn}(j,i) = [E^{sa}_{mn}(j,i)]^{pr} + [E^{sa}_{mn}(j,i)]^{\text{sec}}. \tag{19}$$

The symbol δ_{kl} denotes Kronecker's function. Equation (19) suggests decomposing the term $E^{sa}_{mn}(j,i)$ into a primary and secondary one, in the same way as the spectral Green's dyad in Section II. These terms are given by

$$[E^{sa}_{mn}(j,i)]^{pr(\text{sec})} = \frac{k^2_v}{2\pi}\int_0^\infty dk_x [e^{sa}_{mn}(k_x;j,i)]^{pr(\text{sec})} \tag{20}$$

$$[e^{sa}_{mn}(k_x;j,i)]^{pr(\text{sec})} = Z^{sa}_{mn}(k_x;j,i)\cdot[\gamma^{sa}_{mn}(k_x;j,i)]^{pr(\text{sec})}. \tag{21}$$

The functions $A_{mn}(j), Z^{sa}_{mn}(k_x;j,i)$, that are involved in (18)–(21), are given explicitly in Appendix C. As seen from (20), the terms $[E^{sa}_{mn}(j,i)]^{pr(\text{sec})}$ are defined through infinite spectral integrals. These can be evaluated numerically by restricting the unbounded integration interval $[0,\infty]$ to the finite region $[0,K_x]$, where K_x is a sufficiently large number. At this point, it would be beneficial to search for the asymptotic behavior of the integrands prior to performing the numerical computations. Due to space limitations, we briefly present the conclusions of this analytical investigation. The integrands $[e^{sa}_{mn}(j,i)]^{pr(\text{sec})}$ exhibit a rapidly oscillating behavior, whose amplitude decreases as $1/k^\nu_x$. For the integer number ν it is found that $\nu \geq 2$, and thus the convergence of the integrals is ensured. The weakest convergence, $\nu = 2$, characterizes the primary integrands of (21), when pairs (j,i) of RDW's are considered with $z^j_i = z^j_l$ and $z^j_2 = z^i_2$. Fig. 2 illustrates the configuration of RDW's for which the above conditions holds. Obviously, this also includes the case $j = i$.

The dominant asymptotic expression of $[e^{sa}_{mn}(k_x;j,i)]^{pr}$ is next sought, that applies to the geometry of Fig. 2. Since k_x is assumed to be very large, i.e., $k_x \gg k_0, \beta$, it is plausible to set $\beta = k_i = k^{(i)} = 0$ in those expressions where k_x is also involved. This is equivalent to considering the static case $\omega = 0$ [22]–[23]. Using the above assumptions we find from the expressions shown in Appendix C that the dominant

asymptotic term $[\mathring{e}^{sa}_{mn}(k_x;j,i)]^{pr}$ reads

$$[\mathring{e}^{sa}_{mn}(k_x;j,i)]^{pr} = \frac{2Q^{ji}_{mn}}{k_0^2 k_x^2}[e^{j\phi^{ji}_{mn}}\cos[(\Delta x_{ji}-\ell^-_{ji})k_x] + e^{-j\phi^{ji}_{mn}}\cos[(\Delta x_{ji}+\ell^-_{ji})k_x] - e^{j\psi^{ji}_{mn}}\cos[(\Delta x_{ji}-\ell^+_{ji})k_x] - e^{-j\psi^{ji}_{mn}}\cos[(\Delta x_{ji}+\ell^+_{ji})k_x]]\cdot\eta^{sa} \tag{22}$$

where

$$\eta^{sa} = \begin{cases} -1 & (s,a)=(x,x) \\ 1 & (s,a)=(z,z) \\ 0 & \text{otherwise} \end{cases} \tag{23}$$

and (see Fig. 2)

$$\Delta x_{ji} = x_0^j - x_0^i, \quad \ell^+_{ji} = (\ell^j_x + \ell^i_x)/2, \quad \ell^-_{ji} = (\ell^i_x - \ell^j_x)/2 \tag{24a}$$

$$\phi^{ji}_{mn} = (k^i_{xn}\ell^i_x - (k^j_{xm})^*\ell^j_x)/2,$$
$$\psi^{ji}_{mn} = (k^i_{xn}\ell^i_x + (k^j_{xm})^*\ell^j_x)/2 \tag{24b}$$

$$Q^{ji}_{mn} = e^{-jk^i_{zn}z^i_0}\tilde{f}^z_{j(-m)^*}(-k^i_{zn}). \tag{24c}$$

The function $\tilde{f}^z$ is defined in Appendix C. From (23) it turns out that the $1/k_x^2$ decreasing rate characterizes only the primary terms for $(s,a)=(x,x)$ and (z,z). The analytical investigation presented above can be used to speed-up the numerical evaluation of the integrals. This becomes clear if (20) is rewritten as

$$[E^{sa}_{mn}(j,i)]^{pr} = \frac{k_v^2}{2\pi k_0^2}\left\{\int_0^{k_{x0}} dk_x[e^{sa}_{mn}(k_x;j,i)]^{pr} + \int_{k_{x0}}^{\infty} dk_x[\mathring{e}^{sa}_{mn}(k_x;j,i)]^{pr} + \int_{k_{x0}}^{K_x} dk_x([e^{sa}_{mn}(k_x;j,i)]^{pr} - [\mathring{e}^{sa}_{mn}(k_x;j,i)]^{pr})\right\} \tag{25}$$

and in a more compact form

$$E^{sa}_{mn}(j,i) = E^{sa}_{(1)mn}(j,i) + E^{sa}_{(0)mn}(j,i) + E^{sa}_{(10)mn}(j,i). \tag{26}$$

Thus, the initial integration decomposes into three parts. For the sake of simplicity, indices m,n,s,a,j, and i are suppressed in the following discussion. The lower limit k_{x0} of integration in the terms $E_{(0)}$ and $E_{(10)}$ of (25) is chosen to be equal to k_v. The efficiency of the present method depends critically on the availability of exact forms for the term $E_{(0)}$. Fortunately, this can be computed analytically to give

$$E_{(0)} = \frac{Q^{ji}_{mn}k_v^2}{\pi k_0^2}\{e^{j\phi^{ji}_{mn}}\Lambda(\Delta x_{ji}-\ell^-_{ji},k_{x0}) + e^{-j\phi^{ji}_{mn}}\Lambda(\Delta x_{ji}+\ell^-_{ji},k_{x0}) - e^{j\psi^{ji}_{mn}}\Lambda(\Delta x_{ji}-\ell^+_{ji},k_{x0}) - e^{-j\psi^{ji}_{mn}}\Lambda(\Delta x_{ji}+\ell^+_{ji},k_{x0})\} \tag{27}$$

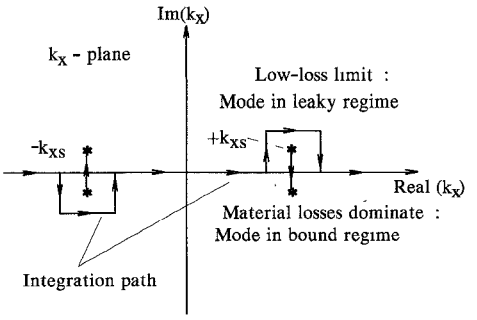

Fig. 3. Integration contour in the complex k_x-plane and migration path from leaky to bound regime of the poles $\pm k_{xs}$, when losses increase.

where we define

$$\Lambda(A,k_{x0}) = \int_{k_{x0}}^{\infty} dk_x \frac{\cos Ak_x}{k_x^2} = \frac{\cos Ak_{x0}}{k_{x0}} - \frac{A\pi}{2} + ASi(Ak_{x0}) \tag{28}$$

and

$$Si(\xi) = \int_0^{\xi}\frac{\sin t}{t}dt. \tag{29}$$

$Si(\xi)$ denotes the sine integral function that can easily be estimated with very small error [24].

To end up with the theoretical examination of the integrals defined in (20), we briefly investigate their pole singularities. The secondary integrands $[e^{sa}_{mn}(k_x;j,i)]^{\text{sec}}$ may have a number of poles that are associated with the roots of the denominators of the reflection coefficients R^{TM} and R^{TE} (Appendix A). These in turn correspond to the TM and TE modes supported by the surrounding [19]. The fundamental substrate mode with propagation constant k_s is the most important to the propagation phenomena in the waveguide. Its associated poles k_{xs} in the complex k_x-plane are given by

$$k^2_{xs} = k_s^2 - \beta^2 \Rightarrow k_{xs} = \pm\sqrt{k_s^2-\beta^2}. \tag{30}$$

It is well known [6], that real propagation constants β of the transmission line are possible only if $\beta > k_s$. Otherwise leakage occurs, resulting in complex wavenumbers β with negative imaginary parts. More rigorously, a transmission line mode is leaky if the following conditions [25] are satisfied

$$\text{Re}(k^2_{xs}) > 0, \quad \text{Im}(k^2_{xs}) \geq 0. \tag{31}$$

The symbol of '=' in the last inequality defines the point where leakage effects turn on. This is seen as the crossing of the real k_x axis by the poles k_{xs} (Fig. 3). In this case, the integration path must be deformed in the complex k_x-plane in order to circumvent the surface wave poles [25], as shown in Fig. 3.

B. Numerical Examples

In order to demonstrate the applicability of the asymptotic extraction technique, as well as its numerical efficiency, we examine a specific waveguide configuration. Consider a single RDW of height $t_{\text{I}} - t_{\text{II}} = 0.45$ cm and width $w = 3$ cm,

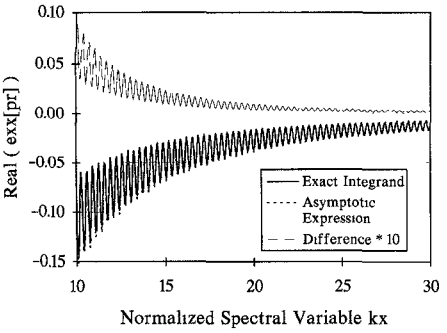

Fig. 4. Plots of the real parts of the integrand $[e_{35}^{xx}(k_x;1,1)]^{pr}$ (solid line), its asymptotic expression (dotted line) and of their difference (dashed line), versus the normalized (to k_v) spectral variable k_x.

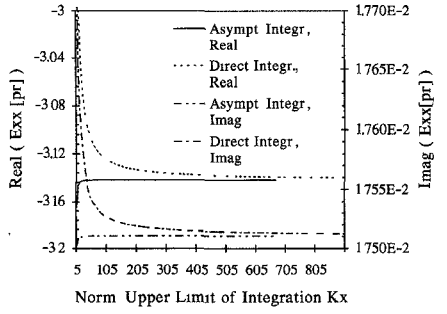

Fig. 5. Comparison between the speeds of convergence of a direct numerical integration and of the asymptotic technique of Section IV for the term $[E_{35}^{xx}(1,1)]^{pr}$ of (25).

which is mounted on a grounded dielectric slab of thickness $t_{\rm II} = 0.38$ cm. This is a special case of the coupled insulated image guides shown in Fig. 6(a), when the separation distance s is zero. To make the example more general, the dielectric materials are assumed lossy with complex permittivities $\varepsilon_g = (2.62 - j0.001)\varepsilon_v$ and $\varepsilon_f = (2.55 - j0.001)\varepsilon_v$ (see Fig. 6(a)). The number of basis functions used is $N_1 = 6$ and the elements of the system matrix are evaluated for the normalized propagation constant $\beta/k_v = 1.57 - j0.0005$. The results presented below, concern the (arbitrary) case $m = 3$ and $n = 5$. Obviously, $j = i = 1$.

Fig. 4 plots the real part of the primary integrand of (21) for $(s,a) = (x,x)$ in the normalized (to the free space wavenumber k_v) region [10–30]. The dominant asymptotic expression of (22) is also depicted and it is essentially indistiguishable from the exact integrand. The dashed line corresponds to their difference multiplied by 10. It is clear that $\mathring{e}(k_x)$ very closely approximates the exact function $e(k_x)$. Consequently, it is anticipated that their difference (term $E_{(10)}$ in (25) and (26)) would be a strongly convergent integral.

Fig. 5 compares the speeds of convergence of the primary integral $[E_{35}^{xx}(1,1)]^{pr}$ between the cases of a usual numerical evaluation and that of the developed asymptotic extraction technique. In the latter case, convergence to the third decimal point is achieved for much smaller values (<40) of the normalized upper limit K_x of integration. Evidently, this contributes to great economy in computation time. The above discussion concerns only the primary term with $(s,a) = (x,x)$. The same conclusions can be inferred for the term

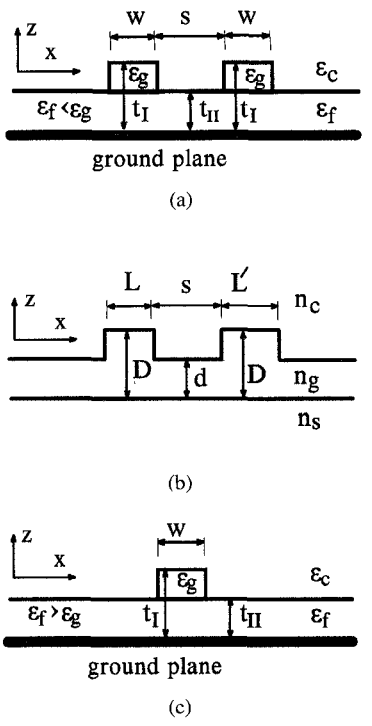

Fig. 6. The waveguide configurations analyzed in the paper: (a) Coupled insulated image guides. (b) Coupled unequal rib guides. (c) Strip dielectric guide.

$(s,a) = (z,z)$, which has a similar asymptotic behavior (see (23)). The remaining primary integrands, as well as all the secondary ones, decrease faster than $1/k_x^3$ and their numerical integration needs no special treatment. Finally, it is pointed out that accurate computation of the elements of the system matrix is of paramount importance in the root seeking process, especially when Muller's method is used to find out solutions in the complex plane.

V. Results and Discussion

The method described above was implemented to calculate propagation constants and fields for the fundamental and higher order modes of several integrated circuits. A first application of this method is given in [16], where a stack of two RDW's is analyzed and the presented results are found to compare very closely to those of a mode matching technique [5]. Additionally, in this paper we examine the structures shown in Fig. 6. The mode nomeclature adopted is that of [1]. Thus, modes are designated as E_{pq}^x if the x component of the electric field dominates and as E_{pq}^z if this is true for the z component. The subindex p and q indicate the number of maxima of the dominant field component in the x and z directions, respectively.

As a first example, we consider the coupled insulated image guides of Fig. 6(a) with parameters: $f = 30.23$ GHz, $t_{\rm I} = 0.83$ cm, $t_{\rm II} = 0.38$ cm. $w = 1.5$ cm, $\varepsilon_g = 2.62\varepsilon_v, \varepsilon_f = 2.55\varepsilon_v$, and $\varepsilon_c = \varepsilon_v$($\varepsilon_v$ denotes the dielectric constant in vacuum). The normalized propagation constants β/k_v of the even and odd E_{11}^z modes are plotted in Fig. 7(a) versus the separation distance s. Both modes are nonleaky, since the wavenumber $k_s/k_v = 1.4918$ of the fundamental TM substrate

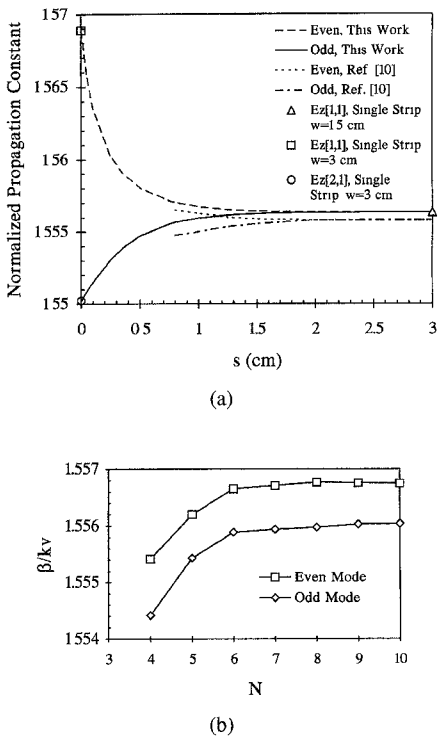

Fig. 7. (a) Normalized propagation constants β/k_v versus the guide separation s of the even and odd E_{11}^z modes of the coupled insulated image guides of Fig. 6(a): $f = 30.23$ GHz, $t_{\rm I} = 0.83$ cm, $t_{\rm II} = 0.38$ cm, $w = 1.5$ cm, $\varepsilon_g = 2.62\varepsilon_v$, $\varepsilon_f = 2.55\varepsilon_v$, and $\varepsilon_c = \varepsilon_v$. (b) Convergence of the results of (a) versus the number N of basis functions for $s = 1$ cm.

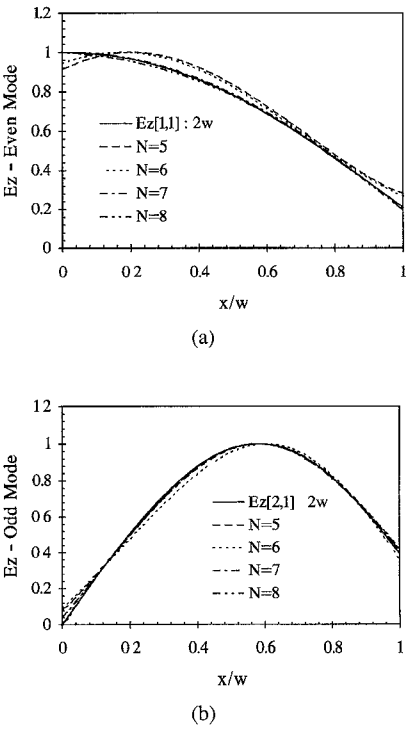

Fig. 8. Normalized z component of the electric field on the right of the coupled RDW's of Fig. 6(a), when $z = (t_{\rm I} + t_{\rm II})/2$ and $s = 0$. (a) Even mode. (b) Odd mode. The solid lines correspond to the (a) E_{11}^z and (b) E_{21}^z field patterns on the right half of a single guide of width $2w = 3$ cm.

mode is less than those in Fig. 7(a). For comparison, the results of [10] are also included in Fig. 7(a). These were obtained using pulse subdomain basis functions. The curves of the present computation appear to be slightly shifted above those of [10]. This discrepancy may be attributed to the different nature of basis function used, as well as to the different computer implementations. However, the maximum relative difference observed is less than 0.1% and consequently the agreement between the methods is considered to be satisfactory.

Fig. 7(b) shows the variation of the propagation constants of Fig. 7(a) versus the number ($N = N_1 = N_2$) of basis functions used, when $s = 1$ cm. In selecting the basis functions, the symmetry of the structure is taken into account, as described in the last paragraph of Section III. It is observed that both modes converge simultaneously. Convergence to within 0.01% is achieved using only 8 basis functions. In this case, the total number of unknowns is $3 \cdot 8 = 24$, reduced to $2 \cdot 8 = 16$ if Gauss' law (15) is applied. Clearly, these numbers are by far smaller than those required in a subsectional basis Galerkin's solution [9]–[10]. The efficiency of the present technique lies in the fact that the unknown field and the entire-domain expansion terms satisfy the same physical laws. Finally, it is pointed out that the results of Fig. 7 can also be obtained without assuming *a priori* any symmetry in the fields, at expense of course of the computation time. This shows another attractive feature of the entire-domain basis function developed: No initial information needs to be provided for the electric field distributions.

An interesting conclusion that can be inferred from Fig. 7(a), is that for small spacings ($s < 1$ cm), the differences of even and odd mode wavenumbers from the single strip propagation constant (marked with a triangle) are not equal, as the coupled mode theory [2] assumes. Furthermore, when s decreases to zero the modes finally end-up to the E_{11}^z and E_{21}^z modes of an insulated image guide of width $2w = 3$ cm. (Note that this case was treated in Section IV where the convergence of the spectral integrals was established). The transition from a configuration of two RDW's to a single one of the double width is seen to be continuous, indicating that the present method can accurately model the dispersion behavior of strongly coupled systems. This will be also demonstrated for the associated field distributions.

Fig. 8 presents the normalized dominant z component of the electric field on the right of the RDW's of Fig. 6(a), when $s = 0$ and $z = (t_{\rm I} + t_{\rm II})/2$. The even mode field distribution is depicted in (a), while the odd one is depicted in (b). In producing these plots, the number of basis functions was increased from $N = 5$ to $N = 8$. Convergence in the field patterns is reached using only 7 basis functions. Fig. 8 also shows the computed (a) E_{11}^z and (b) E_{21}^z field profiles (solid lines) on the right half of a single guide of width $2w = 3$ cm. The latter coincide with the corresponding fields of the even and odd E_{11}^z modes of the coupled system considered above for $s = 0$.

As a next application, the two unequal coupled rib guides of Fig. 6(b) are considered with parameters: $d = 0.9$ μm, $D = 1$ μm, $L = 3$ μm, $L' = 4$ μm, $n_g = 3.44$, $n_s = 3.40$, and $n_c = 1.0$. A wavelength of $\lambda_v = 1.15$ μm is assumed.

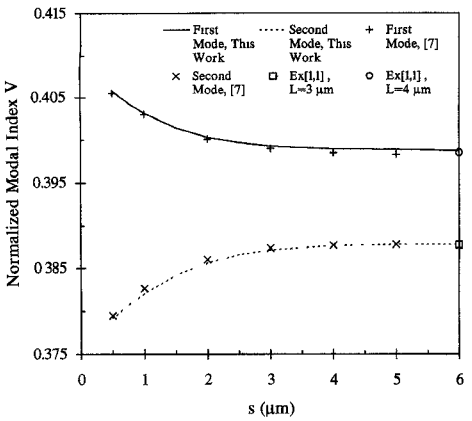

Fig. 9. Variation of the normalized modal indices $V = [(\beta/k_v)^2 - n_s^2]/[n_g^2 - n_s^2]$ of the first two E_{11}^x modes as a function of the guide spacing s for the coupled nonidentical rib guides of Fig. 6(b): $\lambda_v = 1.15\ \mu\text{m}, d = 0.9\ \mu\text{m}, D = 1\ \mu\text{m}, L = 3\ \mu\text{m}, L' = 4\ \mu\text{m}$, $n_g = 3.44$, $n_s = 3.40$, and $n_c = 1.0$.

Fig. 9 shows the variation of the normalized modal indices $V = [(\beta/k_v)^2 - n_s^2]/[n_g^2 - n_s^2]$ of the first two E_{11}^x modes as a function of the guide spacing s. The presented results were derived using 9 basis functions for each RDW and compare very closely to those of a variational method [7]. Since the structure is not symmetric, the modes cannot be divided into even and odd modes. Only if both guides were identical, would these two fundamental modes have even or odd symmetry. For sufficiently large spacing s, the two modes decouple and tend to the E_{11}^x modes of two isolated guides of widths $L = 4\mu$m and $L = 3\ \mu$m, respectively.

As a last example, the authors studied the dispersion characteristics of the strip dielectric waveguide of Fig. 6(c) with parameters $t_{\text{I}} = 0.82$ cm, $t_{\text{II}} = 0.5$ cm, $w = 0.65$ cm, $\varepsilon_g = 2.55\varepsilon_v, \varepsilon_f = 2.62\varepsilon_v$, and $\varepsilon_c = \varepsilon_v$. Fig. 10(a) shows the normalized real parts β_r/k_v and Fig. 10(b) shows the imaginary parts $\log(\alpha/k_v)$ of the propagation constants $\beta = \beta_r - j\alpha$ of the E_{11}^z and E_{11}^x modes, when the free space wavenumber k_v is varied. The fundamental TM and TE substrate modes are also displayed. It is seen that the E_{11}^z mode is bound while the E_{11}^x mode is leaky since its dispersion diagram lies below of that of the TM substrate mode. The results of the present method have been obtained using 7 basis functions and give excellent agreement with results in [10], for both propagation and attenuation constants.

Finally, due to theoretical interest, we investigate the transition of the E_{11}^x mode of Fig. 10 from leaky to bound regime when losses in the materials are introduced. It is assumed that (see Fig. 6(c)) $\varepsilon_{rg} = 2.55(1 - j\tan\delta)$ and $\varepsilon_{rf} = 2.62(1 - j\tan\delta)$, where $\tan\delta$ stands for the loss tangent. The free space wavenumber is fixed at $k_v = 6\ \text{cm}^{-1}$. Fig. 11(a) depicts the variation of the attenuation constants $\log(\alpha/k_v)$ of the modes of Fig. 10, versus $\log(\tan\ \delta)$. It is observed that the attenuation constant of the E_{11}^z mode increases linearly with $\log(\tan\ \delta)$. On the other hand, the attenuation constant of the E_{11}^x mode presents a different behavior. For small material losses ($\log(\tan\ \delta) < -4$) it remains constant indicating that the dominant attenuation mechanism is leakage to the fundamental TM substrate mode. When $\log(\tan\ \delta)$ becomes larger than

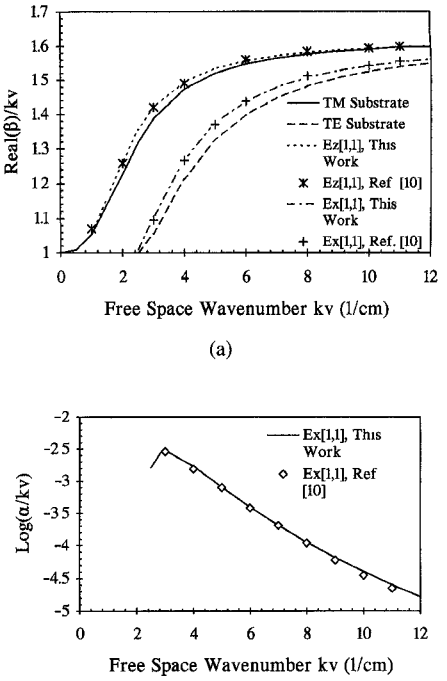

Fig. 10. Dispersion diagrams of the first two modes on the strip dielectric guide of Fig. 6(c): $t_{\text{I}} = 0.82$ cm, $t_{\text{II}} = 0.5$ cm, $w = 0.65$ cm, $\varepsilon_g = 2.55\varepsilon_v, \varepsilon_f = 2.62\varepsilon_v$, and $\varepsilon_c = \varepsilon_v$. (a) Real part β_r/k_v of the propagation constant. (b) Imaginary part $\log(-\text{Im}(\beta)/k_v) = \log(\alpha/k_v)$.

-2, then it increases linearly showing that material losses dominate. In the intermediate region, the E_{11}^x mode turns from leaky to bound state. This is accompanied by the migration of the poles k_{xs} of (30), from the first and third quadrants of the complex k_x plane (Fig. 3) to the fourth and second quadrants, respectively. To study this transition, we plot in Fig. 11(b) the imaginary part $\text{Im}(k_{xs})$ of the corresponding pole k_{xs} on the right half k_x plane, as function of the loss tangent. It is observed that for $\tan\ \delta = 0.01$ this is zero and for larger losses it becomes negative rendering the E_{11}^x mode non leaky. At this point, it should be mentioned that a pole in the first (fourth) quadrant is associated with exponentially increasing (decreasing) fields in the transverse x-direction [11]. For the parameters of Fig. 11, the real part of the pole k_{xs} is almost constant: Re $(k_{xs}) = 0.5742$. The crossing of the real k_x axis by the poles does not cause any trouble in the evaluation of the integrals, provided that the integration path is chosen as in Fig. 3. This transition was shown in the above discussion to be continuous.

VI. Conclusion

An accurate and efficient integral equation analysis of coupled rectangular dielectric waveguides has been presented. The novel concept in this approach lies in the implementation of a proper set of entire-domain basis functions. These functions have the simple form of plane waves and satisfy the appropriate physical laws. In the numerical application of Galerkin's method, an asymptotic extraction technique is employed to speed-up the evaluation of the spectral integrals. For the demonstration of the present method, single and

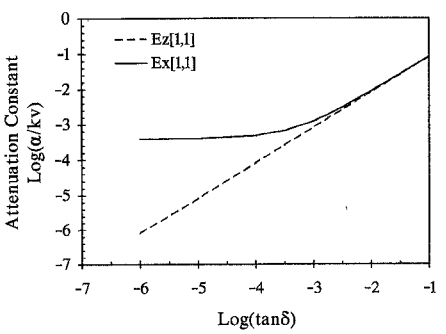

(a)

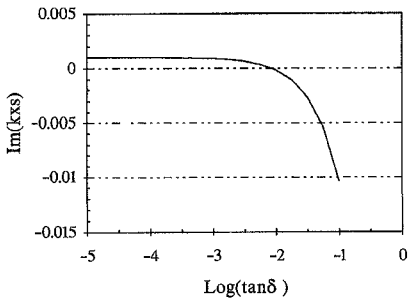

(b)

Fig. 11. Attenuation constants of the modes of Fig. 10, versus $\log(\tan\delta)$ when $\varepsilon_{rg} = 2.55(1-j\tan\delta), \varepsilon_{rf} = 2.62(1-j\tan\delta)$, and $k_v = 6\ \mathrm{cm}^{-1}$. (b) Imaginary part of the pole k_{xs} as function of $\log(\tan\delta)$ and transition from leaky to bound state.

coupled dielectric waveguides are treated for various substrate configurations. Leakage effects in lossy waveguides are also investigated. Where comparisons are available, it is found that this technique yields results which compare very closely to those of other methods.

As revealed through the numerical examples, the expansion set introduced in this paper is global in the sense that it facilitates the modeling of both lossy and lossless guides as well as bound and leaky waves. Even or odd modes can also be specified although non a-priori information on the field distributions is necessary. In addition to the rapid convergence of the spectral integrals, the small number of basis functions (<10) needed to provide accurate results, contributes to a significant reduction in the computation time. The above advantageous features make the proposed set of basis functions very attractive for the modeling of integrated circuits. Further research is being carried out to extend the method to three dimensional structures and anisotropic waveguides.

Appendix A

The reflection coefficients R^{TM} and R^{TE} for the structure of Fig. 1 are given below

$$R^{\mathrm{TM}} = \frac{A_{\mathrm{I}} - B_{\mathrm{I}}}{A_{\mathrm{I}} + B_{\mathrm{I}}} e^{j2k_{z0}d}, \quad R^{\mathrm{TE}} = \frac{C_{\mathrm{I}} + D_{\mathrm{I}}}{C_{\mathrm{I}} - D_{\mathrm{I}}} e^{j2k_{z0}d} \tag{A1}$$

$$A_{\mathrm{I}} = k_{z0}\left[k_{z1}c_1c_2 - \frac{\varepsilon_1}{\varepsilon_2}k_{z2}s_2s_1\right],$$

$$B_{\mathrm{I}} = j\frac{\varepsilon_0}{\varepsilon_1}k_{z1}\left[\frac{\varepsilon_1}{\varepsilon_2}k_{z2}s_2c_1 + k_{z1}c_2s_1\right] \tag{A2}$$

$$C_{\mathrm{I}} = jk_{z0}[k_{z1}s_2c_1 + k_{z2}c_2s_1],$$

$$D_{\mathrm{I}} = k_{z1}[k_{z1}s_2s_1 - k_{z2}c_2c_1] \tag{A3}$$

where

$$k_{zi} = \sqrt{k_i^2 - k_\rho^2}, \quad k_i = \omega\sqrt{\varepsilon_v\mu_v\varepsilon_{ri}}, \quad k_\rho^2 = k_x^2 + k_y^2 \tag{A4}$$

$$s_i = \sin(k_{zi}d_i), \quad c_i = \cos(k_{zi}d_i). \tag{A5}$$

In the case of a structure with semiinfinite substrate (that replaces the ground plane in Fig. 1) of dielectric permittivity ε_3 it is found that

$$R^{\mathrm{TM}} = \frac{A_{\mathrm{II}} - B_{\mathrm{II}}}{A_{\mathrm{II}} + B_{\mathrm{II}}} e^{j2k_{z0}d}, \quad R^{\mathrm{TE}} = \frac{C_{\mathrm{II}} - D_{\mathrm{II}}}{C_{\mathrm{II}} + D_{\mathrm{II}}} e^{j2k_{z0}d} \tag{A6}$$

$$A_{\mathrm{II}} = k_{z0}\left\{k_{z2}\left[\frac{\varepsilon_3}{\varepsilon_0}k_{z1}c_1c_2 - \frac{\varepsilon_1}{\varepsilon_0}\frac{\varepsilon_3}{\varepsilon_2}k_{z2}s_1s_2\right] + jk_{z3}\left[\frac{\varepsilon_2}{\varepsilon_0}k_{z1}c_1s_2 + \frac{\varepsilon_1}{\varepsilon_0}k_{z2}s_1c_2\right]\right\} \tag{A7}$$

$$B_{\mathrm{II}} = k_{z1}\left\{k_{z3}\left[k_{z2}c_1c_2 - \frac{\varepsilon_2}{\varepsilon_1}k_{z1}s_1s_2\right] + jk_{z2}\left[\frac{\varepsilon_3}{\varepsilon_2}k_{z2}c_1s_2 + \frac{\varepsilon_3}{\varepsilon_1}k_{z1}s_1c_2\right]\right\} \tag{A8}$$

$$C_{\mathrm{II}} = k_{z0}\{k_{z2}[k_{z1}c_1c_2 - k_{z2}s_1s_2] + jk_{z3}[k_{z1}c_1s_2 + k_{z2}s_1c_2]\} \tag{A9}$$

$$D_{\mathrm{II}} = k_{z1}\{k_{z3}[k_{z2}c_1c_2 - k_{z1}s_1s_2] + jk_{z2}[k_{z2}c_1s_2 + k_{z1}s_1c_2]\}. \tag{A10}$$

Appendix B

In this Appendix, the (8) of Section III is derived. $\bar{e}_i(x,z)$ denotes the electric field in the ith RDW. We begin with the definition of a Fourier transform pair as

$$\bar{e}_i(x,z) = \frac{1}{(2\pi)^2}\iint_{-\infty}^{\infty} \bar{b}_i(k_x,k_z)e^{jk_xx}e^{jk_zz}\,dk_x\,dk_z \tag{A11}$$

$$\bar{b}_i(k_x,k_z) = \iint_{S_i} \bar{e}_i(x,z)e^{-jk_xx}e^{-jk_zz}\,dx\,dz. \tag{A12}$$

The electric field vector $\bar{e}_i(\bar{\rho})e^{-j\beta y}$ must satisfy the homogeneous Helmholtz's equation for the ith RDW, therefore

$$(\nabla_{x,z}^2 + u_i^2(\beta))\bar{e}_i(x,z) = 0,$$

$$u_i(\beta) = \sqrt{(k^{(i)})^2 - \beta^2}, \quad k^{(i)} = \omega\sqrt{\varepsilon_v\varepsilon_r^{(i)}\mu_v}. \tag{A13}$$

Substitution of (A11) into (A13) gives

$$\iint_{-\infty}^{\infty} (-k_x^2 - k_z^2 + u_i^2(\beta))\bar{b}_i(k_x,k_z) \cdot e^{jk_xx}e^{jk_zz}\,dk_x\,dk_z = 0. \tag{A14}$$

Thus, a non trivial solution can only be obtained if the following condition holds

$$k_x^2 + k_x^2 = u_i^2(\beta). \tag{A15}$$

Equation (A15) suggests writing the spectral variables k_x and k_z as

$$k_x^i(\phi_k) = u_i(\beta)\sin\ \phi_k, \quad k_z^i(\phi_k) = u_i(\beta)\cos\ \phi_k. \quad \text{(A16)}$$

Taking into account the above expressions, the double integral of (A11) is converted into a single one with integration variable the spectral angle ϕ_k. If we introduce a new integration coefficient $\overline{C}_i(\phi_k)$ instead of $\overline{b}_i(\phi_k)$, (A11) transforms to

$$\overline{e}_i(x,z) = \int_0^{2\pi} \overline{C}_i(\phi_k) e^{jk_x^i(\phi_k)(x-x_0^i)} e^{jk_z^i(\phi_k)(z-z_0^i)}\, d\phi_k. \quad \text{(A17)}$$

APPENDIX C

The functions $A_{mn}(j)$, $Z_{mn}^{sa}(k_x;j,i)$, and $\gamma_{mn}^{sa}(k_x;j,i)$ of Section IV are computed here

$$A_{mn}(j) = \iint_{S_j} dx\, dz (f_{jm}^x(x))^* (f_{jm}^z(z))^* f_{jn}^x(x) f_{jn}^z(z)$$
$$= e^{j(k_{zm}^j)^* z_0^j} e^{j(k_{xm}^j)^* x_0^j} \tilde{f}_{jn}^x((k_{xm}^j)^*) \tilde{f}_{jn}^z((k_{zm}^j)^*) \quad \text{(A18)}$$

$$Z_{mn}^{sa}(k_x;j,i) = \zeta_{mn}^{ji}(k_x) \pm \zeta_{mn}^{ji}(-k^x)$$
$$\text{where} \begin{cases} + \text{ for } (s,a) = (x,x),(y,y),(y,z), \\ \qquad\qquad (z,y),(z,z) \\ - \text{ for } (s,a) = (x,y),(x,z),(y,x), \\ \qquad\qquad (z,x) \end{cases} \quad \text{(A19)}$$

$$\zeta_{mn}^{ji}(k_x) = \tilde{f}_{j(-m)^*}^x(-k_x) \cdot \tilde{f}_{in}^x(k_x) \quad \text{(A20)}$$

where we define for $q = x$ or z

$$\tilde{f}_{j(\pm n)^*}^q(\xi) = \frac{e^{j(k_{qn}^j)^* q_0^j}}{j[\pm(k_{qn}^j)^* - \xi]} \cdot \{e^{j[\pm(k_{qn}^j)^* - \xi]q_2^j} - e^{j[\pm(k_{qn}^j)^* - \xi]q_l^j}\}. \quad \text{(A21)}$$

The general expression for the factor $[\gamma_{mn}^{sa}]^{pr}$ is

$$[\gamma_{mn}^{sa}]^{pr}(k_x;j,i) = g_2^{sa}(k_x) I_{2mn}^{ji}(k_x) + g_3^{sa}(k_x) I_{3mn}^{ji}(k_x) \quad \text{(A22)}$$

where

$$I_{2(3)\,mn}^{ji}(k_x) = \int_{z_1^j}^{z_2^j} dz (f_{jm}^z(z))^* e^{\pm jk_{z0}z} \int_{z_1^i}^{z_2^i} dz'\, f_{in}^z(z') \cdot e^{\mp jk_{z0}z'} u(\mp(z-z')). \quad \text{(A23)}$$

Due to the presence of the unit step function $u(\pm(z-z'))$ in the double spatial integral of (A23), the value of $I_{2(3)}$ depends on the relative positions of the RDW's j and i. We consider the following cases for the pair (j,i):

[a] $z_1^j \geq z_2^i$ (RDW no. j is located above RDW no. i)

$$I_{2mn}^{ji}(k_x) = 0, \quad I_{3mn}^{ji}(k_x) = \tilde{f}_{j(-m)^*}^z(k_{z0}) \cdot \tilde{f}_{in}^z(-k_{z0}) \quad \text{(A24)}$$

[b] $z_1^i \geq z_2^j$ (RDW no. j is located below RDW no. i)

$$I_{2mn}^{ji}(k_x) = \tilde{f}_{j(-m)^*}^z(-k_{z0}) \cdot \tilde{f}_{in}^z(k_{z0}), \quad I_{3mn}^{ji}(k_x) = 0 \quad \text{(A25)}$$

[c] $z_2^j = z_2^i, z_1^j = z_1^i$ (Fig. 2)

$$I_{2mn}^{ji}(k_x) = \frac{e^{-jk_{zn}^i z_0^i}}{j[k_{zn}^i - k_{z0}]} \cdot \{e^{j[k_{zn}^i - k_{z0}]z_2^i} \tilde{f}_{j(-m)^*}^z(-k_{z0}) - \tilde{f}_{j(-m)^*}^z(-k_{zn}^i)\} \quad \text{(A26)}$$

$$I_{3mn}^{ji}(k_x) = \frac{e^{-jk_{zn}^i z_0^i}}{j[k_{zn}^i + k_{z0}]} \{-e^{j[k_{zn}^i + k_{z0}]z_1^i} \tilde{f}_{j(-m)^*}^z(k_{z0}) + \tilde{f}_{j(-m)^*}^z(-k_{zn}^i)\}. \quad \text{(A27)}$$

Finally, the secondary term $[\gamma_{mn}^{sa}]^{\text{sec}}$ is given by

$$[\gamma_{mn}^{sa}]^{\text{sec}}(k_x;j,i) = g_1^{sa}(k_x) I_{1mn}^{ji}(k_x),$$
$$I_{1mn}^{ji}(k_x) = \tilde{f}_{j(-m)^*}^z(k_{z0}) \cdot \tilde{f}_{in}^z(k_{z0}). \quad \text{(A28)}$$

REFERENCES

[1] E. A. J. Marcatili, "Dielectric rectangular waveguide and directional coupler for integrated optic," *Bell Syst. Tech. J.*, vol. 48, pp. 2071–2102, Sept. 1969.

[2] T. Tamir, Ed., *Guided-Wave Optoelectronics.* Berlin: Springer-Verlag, 1990.

[3] L. P. B. Katehi, "Novel transmission lines for the submillimeter-wave region," in *Proc. IEEE,* vol. 80, Nov. 1992, pp. 1771–1787.

[4] B. M. A. Rachman and J. B. Davies, "Finite-element solution of integrated optical waveguides," *J. Lightwave Tech.,* vol. 2, pp. 682–688, Oct. 1984.

[5] A. G. Engel and L. P. B. Katehi, "Low-loss monolithic transmission lines for sub-mm and Terahertz frequency applications," *IEEE Trans. Microwave Theory Tech.,* vol. 39, pp. 1847–1854, Nov. 1991.

[6] S. T. Peng and A. A. Oliner, "Guidance and leakage properties of a class of open dielectric waveguides: Part I: Mathematical formulations," *IEEE Trans. Microwave Theory Tech.,* vol. MTT-29, pp. 843–855, Sept. 1981.

[7] T. Rozzi, M. N. Husain, and L. Zappelli, "Rigorous analysis of multiple coupled rib waveguide," *IEEE Trans. Microwave Theory Tech.,* vol. 40, pp. 706–715, Apr. 1992.

[8] J. S. Bagby, D. P. Nyquist, and B. C. Drachman, "Integral formulation for analysis of integrated dielectric waveguides," *IEEE Trans. Microwave Theory Tech.,* vol. MTT-33, pp. 906–915, Oct. 1985.

[9] E. W. Kolk, N. H. G. Baken, and H. Blok, "Domain integral equation analysis of integrated optical channel and ridge waveguides in stratified media," *IEEE Trans. Microwave Theory Tech.,* vol. 38, pp. 78–84, Jan. 1990.

[10] J. F. Kiang, S. M. Ali, and J. A. Kong, "Integral equation solution to the guidance and leakage properties of coupled dielectric strip waveguides," *IEEE Trans. Microwave Theory Tech.,* vol. 38, pp. 193–203, Feb. 1990.

[11] F. Olyslager and D. De Zutter, "Rigorous boundary equation solution for general isotropic and uniaxial anisotropic dielectric waveguides in multilayered media including losses, gain, and leakage," *IEEE Trans. Microwave Theory Tech.,* vol. 41, pp. 1383–1392, Aug. 1993.

[12] K. Sabetfakhri and L. P. B. Katehi, "An integral transform technique for analysis of planar dielectric structures," *IEEE Trans. Microwave Theory Tech.,* vol. 42, pp. 1052–1062, June 1994.

[13] H. Y. Yang, J. A. Castaneda, and N. G. Alexopoulos, "An integral equation analysis of an infinite array of rectangular dielectric waveguides," *IEEE Trans. Microwave Theory Tech.,* vol. 38, pp. 873–880, July 1990.

[14] M. Viola and D. Nyquist, "An electric field integral equation for the transverse field components within integrated dielectric waveguides," *J. Electromagnetic Waves and Applications,* vol. 5, no. 11, pp. 1283–1297, 1991.

[15] P. G. Cottis and N. K. Uzunoglu, "Integral equation approach for the analysis of anisotropic channel waveguides," *J. Opt. Soc. Am. A.,* vol. 20, pp. 608–614, Apr. 1991.

[16] G. Athanasoulias and N. K. Uzunoglu, "An entire-domain basis Galerkin's method for the modeling of integrated mm-wave and optical circuits," in *IEEE MTT-S Dig.,* May 1995, pp. 471–474.

[17] A. D. Yaghjian, "Electric dyadic Green's function in the source region," in *Proc. IEEE,* vol. 68, Feb. 1980, pp. 248–263.

[18] W. C. Chew, "Some observations on the spatial and eigenfunction representation of the dyadic Green's function," *IEEE Trans. Antennas Propagat.,* vol. 37, pp. 1322–1327, Oct. 1989.

[19] S. Barkeshli and P. H. Pathak, "On the dyadic Green's functions for a planar multilayered dielectric/magnetic media," *IEEE Trans. Microwave Theory Tech.*, vol. 40, pp. 128–142, Jan. 1992.
[20] A. Ishimaru, *Electromagnetic Wave Propagation, Radiation, and Scattering.* London: Prentice Hall, 1991.
[21] E. T. Whittaker and G. N. Watson, *A Course of Modern Analysis.* Cambridge: Cambridge Univ. Press, 1969, Chap. XVIII.
[22] P. B. Katehi and N. G. Alexopoulos, "Real axis integrations of Sommerfeld integrals with application to printed circuit antennas," *J. Math. Phys.*, vol. 24, no. 3, pp. 527–533, Mar. 1983.
[23] T. Itoh, Ed., *Numerical Techniques for Microwave and Millimeter-Wave Passive Structures.* New York: Wiley, 1989, Ch. 3.
[24] M. Abramowitz and I. A. Stegun, *Handbook of Mathematical Functions.* New York: Dover, 1970.
[25] J. Bagby, C. H. Lee, D. P. Nyquist, and Y. Yuan, "Identification of propagation regimes on integrated microstrip transmission lines," *IEEE Trans. Microwave Theory Tech.*, vol. 41, pp. 1887–1893, Nov. 1993.

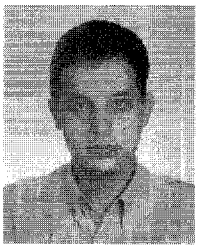

G. Athanasoulias (S'93) was born in Tripolis, Greece, in 1968. He received the Diploma degree (with distinction) in electrical engineering from the National Technical University of Athens (NTUA) in 1990, and the M.Sc. degree by research in electronic systems engineering from the University of Essex, UK, in 1991. He is currently completing the Ph.D. degree in the Department of Electrical and Computer Engineering of NTUA.

His research interests include analytical and numerical methods in electromagnetics, propagation of EM waves in atmosphere, microwave circuits, and guidance and leakage phenomena in integrated mm-wave and optical circuits.

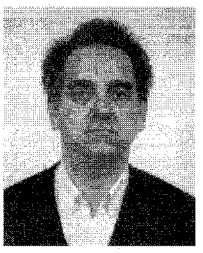

N. K. Uzunoglu (M'82) was born in Constantinopole in 1951. He received the B.Sc. degree in electronics from the Technical University of Istanbul in 1973, and the M.Sc. and Ph.D. degrees in 1974 and 1976, respectively, from the University of Essex.

He worked from 1977 to 1984 as a Research Scientist at the Office of Research and Technology of the Hellenic Navy. In 1984 he was elected Associate Professor at the Department of Electrical Engineering, National Technical University of Athens (NTUA), and in 1987 he was promoted to Professor. In 1986 he was elected Vice-Chairman of the Department of Electrical Engineering, NTUA, and in 1988 he was elected Chairman of the same department. He was reelected as Chairman in 1992. In 1991 he was elected and appointed Director of the Institute of Communications and Computer Systems, an independent research establishment associated with NTUA. His research interests include electromagnetic scattering, radiation phenomena, propagation of electromagnetic waves in atmosphere, medical applications of electromagnetic waves, fiber optics telecommunications, and high-speed circuits operating at Gb/s rates.

Dr. Uzunoglu received the International G. Marconi Award in Telecommunications in 1981. Since 1988 he has been the National Representative of Greece to the COST, Technical Telecommunications Committee, actively participating in several COST projects. Further, he has been Project Manager in several RACE, ESPRIT, and National research and development projects in the fields of telecommunications and biomedical engineering. He has 100 publications in refereed international journals, and he published three books in Greek on microwaves, fiber optics telecommunications, and radar systems.